

Metabolic Reprogramming of Macrophages Exposed to Silk, Poly(lactic-co-glycolic acid), and Silica Nanoparticles

Raquel Saborano, Thidarat Wongpinyochit, John D. Totten, Blair F. Johnston, F. Philipp Seib,* and Iola F. Duarte*

Monitoring macrophage metabolism in response to nanoparticle exposure provides new insights into biological outcomes, such as inflammation or toxicity, and supports the design of tailored nanomedicines. This paper describes the metabolic signature of macrophages exposed to nanoparticles ranging in diameter from 100 to 125 nm and made from silk, poly(lactic-co-glycolic acid) or silica. Nanoparticles of this size and type are currently at various stages of preclinical and clinical development for drug delivery applications. ¹H NMR analysis of cell extracts and culture media is used to quantify the changes in the intracellular and extracellular metabolomes of macrophages in response to nanoparticle exposure. Increased glycolytic activity, an altered tricarboxylic acid cycle, and reduced ATP generation are consistent with a proinflammatory phenotype. Furthermore, amino acids possibly arising from autophagy, the creatine kinase/phosphocreatine system, and a few osmolytes and antioxidants emerge as important players in the metabolic reprogramming of macrophages exposed to nanoparticles. This metabolic signature is a common response to all nanoparticles tested; however, the direction and magnitude of some variations are clearly nanoparticle specific, indicating material-induced biological specificity. Overall, metabolic reprogramming of macrophages can be achieved with nanoparticle treatments, modulated through the choice of the material, and monitored using ¹H NMR metabolomics.

1. Introduction

The concept of nanoparticle-based drug delivery dates back to the 1970s, but Abraxane was the first drug delivery nanoparticle to reach routine clinical use in 2005. Over the past decade, new concepts for nanoparticle-based therapies have emerged; for example, the combination of both therapeutic and diagnostic capabilities in a single carrier (i.e., theranostics).^[1] Today, numerous nanoparticles are in clinical development for a broad range of indications, including hypercholesterolemia, seasonal influenza, diabetes, smoking cessation, and cancer.^[2] Nanoparticles designed for the treatment of solid tumors are typically in the 100 nm size range and exploit the leaky vasculature and reduced lymphatic drainage of tumors to achieve passive targeting,^[3] a phenomenon known as the “enhanced permeation and retention” effect.^[4] The use of active targeting moieties can promote further increases in drug concentrations within the tumor.

However, tumor-associated macrophages, as well as professional macrophages in the blood, liver (Kupfer cells), lung (alveolar macrophages), and spleen, are key contributors to nanoparticle clearance. This clearance is a major problem for nanoparticles designed for intracellular targeting of tumor cells because it diverts them from their intended sites of action, resulting in increased side effects, diminished therapeutic efficacy and, indeed, a potentially adverse tumor response. For example, nanoparticle-induced C5a anaphylatoxin increases macrophage uptake^[5] as well as stimulates tumor growth by suppressing CD8+ T cells.^[6] Conversely, targeting tumor-associated macrophages^[7,8] or exploiting particulate-mediated immune modulation can be used to manipulate the tumor microenvironment or to moderate (cancer-associated) inflammatory responses, respectively.^[9] Thus, an appropriate design and assessment of the (nano)particle is necessary to achieve the intended biological outcome; this includes the metabolic assessment of macrophage responses to nanoparticles.

Recent findings have established metabolic reprogramming as a key element of the functional behavior of macrophages, so that metabolism is now viewed as more than just energy generation and biosynthesis.^[10,11] In particular, the activation of macrophages by different environmental signals (e.g.,


R. Saborano, Dr. I. F. Duarte
CICECO – Aveiro Institute of Materials
Department of Chemistry
University of Aveiro
3810-193 Aveiro, Portugal
E-mail: ioladuarte@ua.pt

T. Wongpinyochit, J. D. Totten, Dr. B. F. Johnston, Dr. F. P. Seib
Strathclyde Institute of Pharmacy and Biomedical Sciences
University of Strathclyde
161 Cathedral Street, Glasgow G4 0RE, UK
E-mail: philipp.seib@strath.ac.uk

Dr. F. P. Seib
Leibniz-Institut für Polymerforschung Dresden e.V.
Max Bergmann Centre of Biomaterials Dresden
Hohe Strasse 6, 01069 Dresden, Germany

This is an open access article under the terms of the Creative Commons Attribution License, which permits use, distribution and reproduction in any medium, provided the original work is properly cited.

The copyright line for this article was changed on 18 May 2017 after original online publication.

 The ORCID identification number(s) for the author(s) of this article can be found under <https://doi.org/10.1002/adhm.201601240>.

DOI: 10.1002/adhm.201601240

lipopolysaccharide and interleukins, resulting in M1 and M2 macrophages, respectively) has a known association with marked alterations in cellular metabolism.^[12,13] These alterations can ideally be followed using metabolomics, as this approach permits the unbiased and simultaneous detection of a wide range of cellular metabolites in response to a stimulus, including nanoparticles.^[14] High resolution nuclear magnetic resonance (NMR) is an exquisite and extremely powerful tool for metabolomics, despite its inherent sensitivity limitations. NMR shows unparalleled analytical reproducibility and imparts the ability to obtain unequivocal structural and quantitative information on metabolites involved in central metabolic pathways. NMR-based metabolomics is well established in disease profiling and drug development studies,^[15] and the literature reporting the use of this technique for assessment of cellular responses to nanoparticles continues to increase (reviewed by Lv and co-authors).^[16] However, the metabolic responses of macrophages to nanoparticles are poorly characterized and, to our knowledge, the only previous study examining macrophage metabolomic changes was conducted with ultrasmall iron oxide nanoparticles.^[17]

Here, we use NMR metabolomics to assess the impact of different nanoparticles on macrophage metabolism, to uncover nanoparticle-induced metabolic activation profiles. For this study, we have selected three types of nanoparticles [made from silk, poly(lactic-co-glycolic acid) (PLGA), or silica] with diameters within a 100–125 nm size range; these types of nanoparticle are presently at various stages of preclinical and clinical development for biomedical applications (e.g., solid tumor targeting, smoking cessation^[2]). While silk nanoparticles have been recently proposed as promising drug delivery platforms,^[18] nanoparticles made of PLGA (a synthetic polymer approved for human use by Food and Drug Administration and European Medicines Agency) are among the most successful vectors for delivery of biomolecules and drugs in the clinical setting.^[19] On the other hand, silica nanoparticles are being increasingly explored for both drug delivery and bioimaging applications.^[20] We have used RAW 264.7 macrophages for this study because this cell line has emerged as a valuable model for assessing macrophage responses to various stimuli, and their use permits direct comparison to other studies.^[21–26] The changes in the intracellular and extracellular metabolomes of macrophages, at different nanoparticle concentrations and exposure times, were assessed by ¹H NMR analysis of cell extracts and culture media.

2. Results

2.1. Impact of Nanoparticles on Cellular Morphology and TNF- α Release

Qualitative scanning electron microscopy studies were performed on both nanoparticle preparations (Figure 1a) and nanoparticle exposed cells (Figure 1b); all nanoparticles were spherical, uniform and of the expected size. Cells exposed to nanoparticle preparations at selected concentrations showed substantial differences. Cells were tightly “coated” by silica and silk nanoparticles. Furthermore, silk nanoparticles, besides their tight coating behavior, also showed “loose” packing

(Figure 1b, asterisk). Cells exposed to PLGA nanoparticles showed no signs of cell coating, instead showing loose packing around the cells (Figure 1b). Loose nanoparticle packing was never observed for silica nanoparticles in any of the examined samples. However, for silk and PLGA nanoparticles, this loose packing was often lost during sample preparation (data not shown), suggesting that these structures were fragile. Higher resolution images showed substantial interaction of silica and silk nanoparticles with the plasma membrane of the RAW 264.7 cells (Figure 2a,b). Cells exposed to silk nanoparticles showed a range of cell morphologies including a migratory phenotype, with signs of lamellipodium formation (Figure 2b closed arrow) and membrane ruffles (Figure 2b open arrow); these features were absent in the silica-treated cells. Cells exposed to nanoparticles at 10 $\mu\text{g mL}^{-1}$ showed similar morphologies for all treatment groups (Figure S1, Supporting Information) and were indistinguishable from the control cells (Figure 1b).

The TNF- α release was measured in conditioned medium following exposure of RAW 264.7 cells to nanoparticles (Figure 2d). Treatment with any of the nanoparticles at 10 $\mu\text{g mL}^{-1}$ caused no significant change in TNF- α release when compared to control cultures. However, a silica nanoparticle concentration of 500 $\mu\text{g mL}^{-1}$ triggered the highest TNF- α release. Significantly lower release was measured for cells treated with PLGA nanoparticles and release was even lower for cells treated with silk nanoparticles ($P < 0.01$ for PLGA versus silk). The response of RAW 264.7 cells to lipopolysaccharide was used as a positive control. Scanning electron microscopy imaging showed that lipopolysaccharide activation and subsequent TNF- α release was not coupled to changes in cell morphology (Figure 2c,d).

2.2. Impact of Nanoparticles on the Intracellular Metabolome

A typical ¹H NMR spectrum of macrophage aqueous extract (Figure 3) shows contributions from several tens of metabolites, from which nearly 40 were unequivocally identified (Table S1, Supporting Information). Principal component analysis (PCA) was applied to the spectra to explore data and grouping trends. The main sources of variability accounting for sample distribution in the resulting scores scatter plot (Figure 4) were culture time and nanoparticle concentration. Indeed, sample scores along PC1, which explained 30% of the variance, were related to culture time, with 24 h samples clustering together in negative PC1 and separating from the 48 and 72 h samples (Figure 4a). PC2 (explaining 22% of the variance) separated samples exposed to the high nanoparticle concentration (positive PC2) from the controls and the samples exposed to the low nanoparticle concentration (negative PC2) (Figure 4b). No clustering according to nanoparticle type was apparent, regardless of the PCs being considered.

As culture time appeared to be a key factor, multivariate modeling was conducted for each individual time point. The PCA score plots (Figure S2, Supporting Information) allowed two observations, namely (i) the samples exposed to low nanoparticle concentrations overlapped with controls at all times, while separating from high concentration samples along PC1; and (ii) a trend was observed for sample separation according

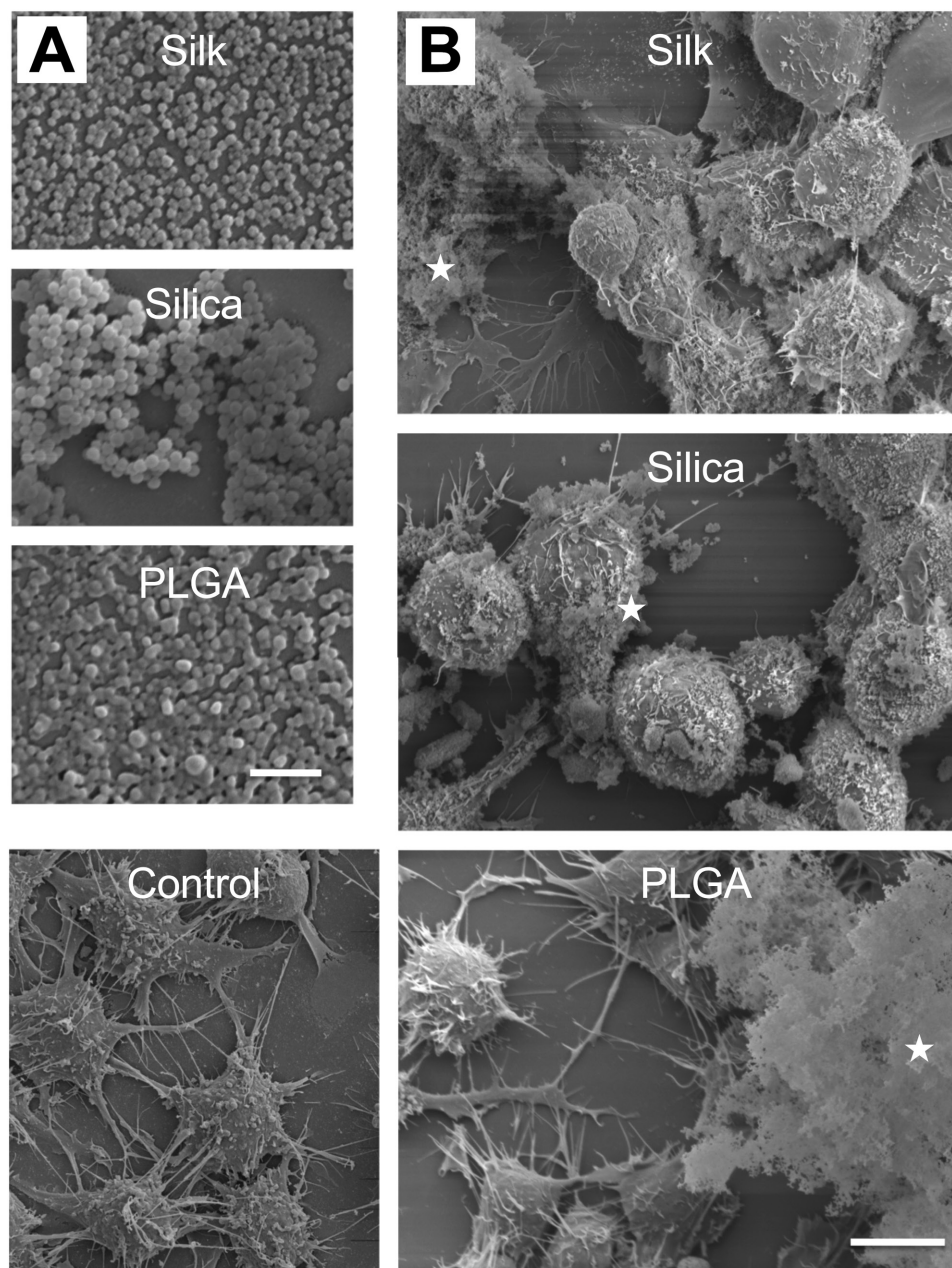


Figure 1. Representative scanning electron micrographs of nanoparticles and cells. a) Nanoparticles (scale bar: 500 nm) and b) RAW 264.7 cells exposed to nanoparticles ($500 \mu\text{g mL}^{-1}$) after a 24 h exposure. Asterisks denote examples of nanoparticle coatings that loosely (PLGA and silk) and tightly (silica) wrap the cells (scale bar: $10 \mu\text{m}$).

to nanoparticle type, especially at 72 h, where, with the exception of one PLGA sample, three distinct clusters appeared for silk, PLGA, and silica nanoparticle-exposed samples, separated along PC4.

These PCA results were used to construct partial-least squares discriminant analysis (PLS-DA) models for individual time points and each nanoparticle type, considering two classes—control and high nanoparticle concentration—in order to highlight nanoparticle-specific metabolic variations. The low concentration samples were not considered further, as their metabolic profiles were very similar to the controls. The PLS-DA

scores and loading plots obtained for 24 h samples are shown in **Figure 5**; the results for 48 and 72 h samples are presented in Figures S3 and S4 (Supporting Information). In all cases, the controls were clearly discriminated from nanoparticle-exposed samples with high robustness ($Q^2 > 0.5$). Inspection of the loadings explaining sample discrimination along the first latent variable (LV1) allowed ready identification of the main metabolic differences. The 24 h exposure showed loading profiles (Figure 5, left) indicating that some effects, such as increases in creatine and phosphocreatine (red-negative loadings) and decreases in aspartate, betaine, and myo-inositol (red-positive

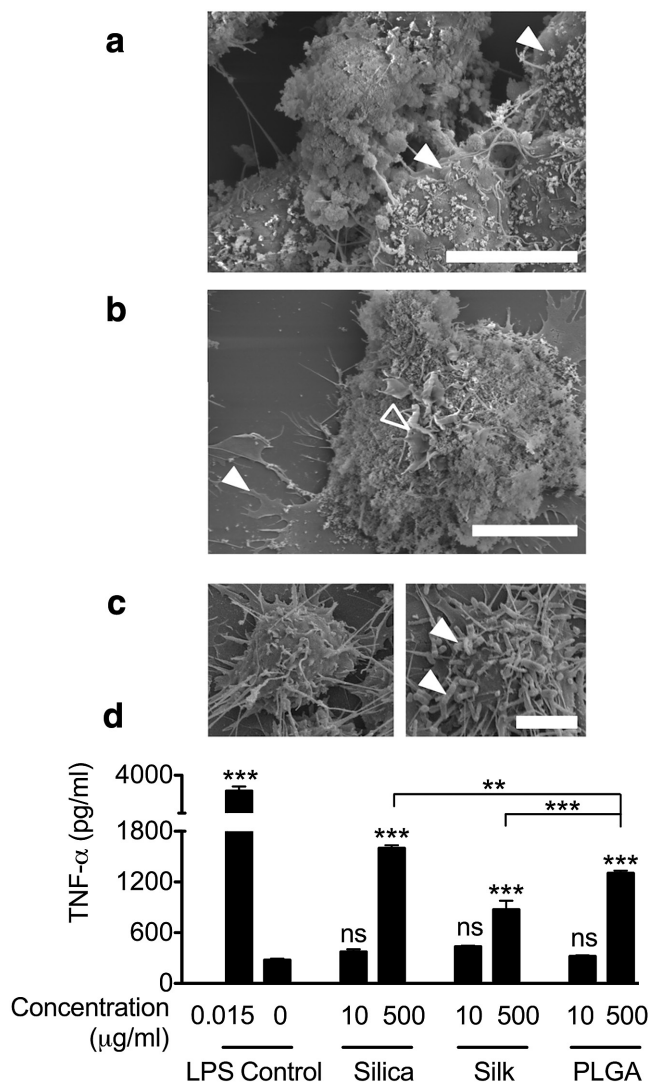


Figure 2. Macrophage response to nanoparticles. Representative scanning electron micrographs of RAW 264.7 cells exposed to a) silica and b) silk nanoparticles for 24 h (scale bar: 10 μm). Closed arrows denote the exposed cell plasma membrane. Silica and silk nanoparticles extensively covered the cells with some visible membrane ruffles (silk, open arrow). c) Examples of control cells (left panel) and cells exposed to lipopolysaccharide (LPS) (arrows) (right panel) (scale bar: 5 μm). d) Tumor necrosis factor alpha (TNF-α) release into the cell culture medium following a 24 h exposure to nanoparticles. Statistical analysis included an ANOVA followed by Bonferroni's multiple comparison post hoc test (bars above samples) and Dunnett's post hoc test using the control sample as a reference point ($n = 3, \pm \text{SD}$).

loadings), were common to the three nanoparticle types. However, some variations appeared to be nanoparticle-specific. For instance, an increase in glutamine was only observed for silica nanoparticles, whereas glycine showed opposite variations in silk and silica nanoparticle-exposed cells. The loading profiles for 48 and 72 h shared many common features with the 24 h data sets, though a few additional material-specific variations were evident at the later time points (e.g., phosphocholine, glycerophosphocholine; Figures S3 and S4, Supporting Information).

Spectral integration results were summarized in a heatmap showing the percentage variation to assess the magnitude and significance of differences in individual metabolites for each exposure time and nanoparticle type when compared to controls (Figure 6 and Table S2, Supporting Information). Only the metabolites with a representative large effect size (i.e., absolute value >0.8, justified in ref. [27]) were included.

All nanoparticles caused significant changes in metabolites involved in glycolysis and the tricarboxylic acid (TCA) cycle. In particular, pyruvate was decreased in cells exposed to silk nanoparticles (up to 30%), while lactate was increased in all treated cells (up to 284% in cells exposed to silk and up to 182% and 131% in cells exposed to PLGA and silica nanoparticles, respectively). Itaconate and succinate were also increased, particularly in cells exposed to PLGA nanoparticles.

The intracellular levels of several amino acids were altered in macrophages exposed to nanoparticles. Aspartate, glutamate, alanine, and threonine were consistently decreased in exposed samples, regardless of nanoparticle type (blue patches in the heatmap, Figure 6). By contrast, lysine, branched chain amino acids (valine, leucine, isoleucine) and aromatic amino acids (tyrosine, phenylalanine) showed time-dependent increases, which were generally of higher magnitude in cells incubated with silk nanoparticles than with other nanoparticles (orange/red patches in the heatmap, Figure 6). The variations in glutamine and glycine were clearly dependent on nanoparticle type. Glutamine increased significantly in cells exposed to silica nanoparticles for 24 h, followed by normalized levels at longer exposure periods. Silk nanoparticle exposure caused a transient glutamine decrease at 48 h, while PLGA nanoparticle exposure had no effect on glutamine levels. Alterations in glycine included a decrease at 24 h in response to silica nanoparticles and substantial increases at 48 h with silk and PLGA nanoparticles.

The levels of energy-related metabolites were greatly affected in nanoparticle exposed cells. Cellular ATP decreased following exposure to all nanoparticle types for 48 h or longer, while significant increases in creatine (69% to 541%) and phosphocreatine (36% to 482%) were evident, especially for the shorter exposure times. Comparison of the three nanoparticle types revealed that silk and silica nanoparticles produced the greatest change in creatine and phosphocreatine levels, with lesser changes occurring in the cells treated with PLGA nanoparticles. Indeed, after a 72 h exposure to PLGA nanoparticles, the intracellular levels of creatine and phosphocreatine were, respectively, similar or lower relative to controls, highlighting the time-dependent and dynamic nature of the metabolome changes.

Other prominent variations included a consistent decrease in myo-inositol, together with time- and material-dependent variations in choline compounds, taurine and betaine. Phosphocholine and glycerophosphocholine decreased in macrophages exposed to silk or silica nanoparticles, while PLGA nanoparticles promoted an increase in glycerophosphocholine and no change in phosphocholine. Taurine and betaine showed reduced levels in cells exposed to PLGA or silica nanoparticles for 24 h, but increased if exposure was increased to 72 h.

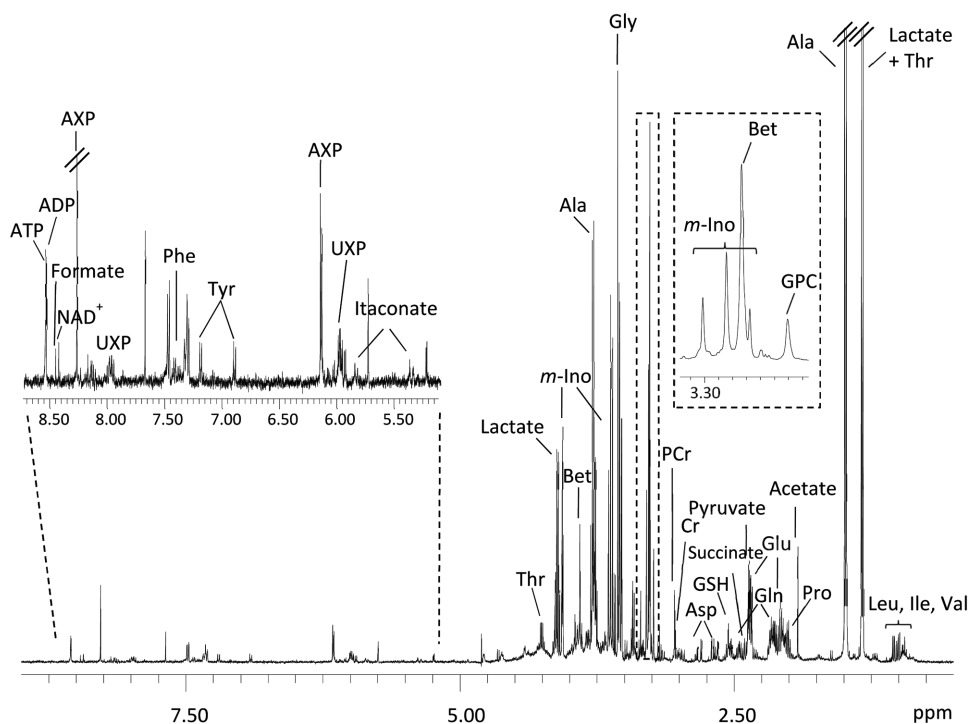


Figure 3. 500 MHz ^1H NMR spectrum of an aqueous extract from RAW 264.7 control cells. Some assignments are indicated: three-letter code used for amino acids, ADP adenosine diphosphate, ATP adenosine triphosphate, AXP (ADP/ATP), Bet betaine, Cr creatine, GPC glycerophosphocholine, GSH reduced glutathione, *m*-Ino myo-inositol, NAD^+ oxidized nicotinamide adenine dinucleotide, PC phosphocholine, PCr phosphocreatine, UXP (UDP/UTP uridine diphosphate/ uridine triphosphate).

2.3. Impact of Nanoparticles on the Extracellular Metabolome

The cellular metabolism of macrophages exposed to nanoparticles was further analyzed by measuring cell-mediated variations in the culture medium composition (Figure 7; Table S3, Supporting Information). Compared to control cells, macrophages exposed to nanoparticles for 48 h or longer consumed more glucose, thereby decreasing the glucose levels in their respective media. Lactate and itaconate excretion was also higher from exposed cells than from control cells, whereas the release of pyruvate was significantly reduced in cells exposed for 72 h. Citrate excretion was also lower at the same exposure duration, except for macrophages exposed to silica nanoparticles, where citrate levels remained comparable to those of the control cells.

The conditioning medium surrounding exposed cells differed from the control medium with respect to the levels of several amino acids. The control cells consumed glutamine, valine, leucine, isoleucine, and methionine, unlike nanoparticle exposed cells; especially at the 24 h time point, silica nanoparticles induced hydrolysis/consumption of alanyl-glutamine coupled with the corresponding large increases in free extracellular alanine and glutamine (which also increased inside the cells). Extracellular alanine further increased at 48/72 h, indicating its increased excretion by exposed cells. Glycine excretion, on the other hand, only increased in the medium of cells exposed to silk nanoparticles. Note, however, that incubation of medium alone with silk nanoparticles (without cells) did not result in any change in glycine levels. A few amino acids

showed invariant levels in control cells (neither consumed nor excreted) but increased their levels in the conditioning medium when the cells were exposed to nanoparticles; these were threonine, lysine, tyrosine, and phenylalanine.

Overall, the nanoparticles-modulated macrophage metabolism that was indicative of the M1-like phenotype.^[13,28] Therefore surface expression of CD80 and cytokine production in response nanoparticles was assessed (Figure 8a,b).^[29] All nanoparticles induced the plasma membrane expression of CD80, with similar levels observed for silica and silk (25% of CD80 positive cells) and significantly higher levels for PLGA (39% of CD80 positive cells); lipopolysaccharide (LPS) served as the positive control (>90% CD80 positive cells). Conditioned cell culture medium from nanoparticle-treated and LPS-treated cells showed upregulation of (proinflammatory) cytokines (Figure 8c). For example, all nanoparticles and LPS induced substantial increases in IL-1ra, CCL3, and CCL4, but the nanoparticles failed to increase GM-CSF, IL10, and IL6 above the detection limit of this assay.

3. Discussion

Nanoparticles can be delivered into the body using a range of administration routes (e.g., intravenous, inhaled, subcutaneous, etc.), with the view of evoking the desired therapeutic response. Targeting specific macrophage populations could be part of a therapeutic strategy, or it could simply be an inadvertent consequence of a serendipitous nanoparticle design. Macrophage

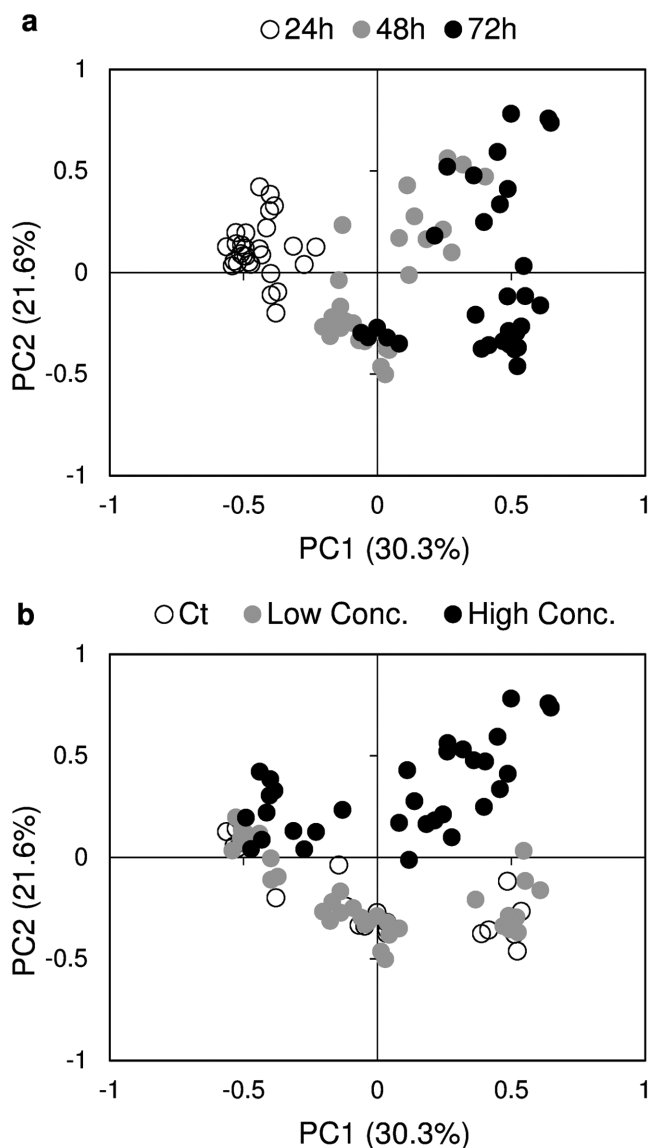


Figure 4. Scores scatter plots resulting from applying PCA to the ¹H NMR spectra from cell aqueous extracts: a) scores colored by culture time and b) scores colored by nanoparticle concentration.

responses toward nanoparticles depend on multiple factors; these include, but are not limited to, the bulk material and surface modification (chemical and/or physical), as well as particle size, geometry, exposure time, and dose (reviewed in ref. [30]). Thus, selecting synthetic, inorganic, and biopolymer based nanoparticles for comparative metabolomic assessment can be challenging and, to the best of our knowledge, has not been attempted before.

In this study, we assessed nanoparticles that were in the 100 nm size range because clinically approved (e.g., Abraxane, 130 nm) and emerging (e.g., Bind-014, 100 nm, developed by BIND Therapeutics) nanoparticles for anticancer drug delivery are all within this size range.^[1,31] Furthermore, particles in the 100 nm size range are also capable of efficiently exploiting the enhanced permeation and retention effect for passive tumor

targeting.^[3] The maximum dose (500 $\mu\text{g mL}^{-1}$) and 72 h exposure time were selected to emulate the clinical pharmacokinetics observed with synthetic nanoparticles in man.^[31] In the current study, we worked with nanoparticles made from PLGA, silica, and silk. We selected PLGA because many nanoparticles currently in clinical development use this synthetic polymer;^[2,19] furthermore, PLGA has a track record for use in humans. Silica was selected as an inorganic material. Although there is much excitement about the perceived benefit(s) of silica for nanomedicine applications,^[20,32] its track record is controversial. Previous *in vitro* and *in vivo* studies have indicated that silica nanoparticles can readily induce toxicity and alter cellular metabolism.^[33–36] In addition to the synthetic polymer and the inorganic material, we included the biopolymer silk.^[37] Over the past decade, silk has emerged as a promising contender for drug delivery applications.^[18,38,39] First, silk has a track record for use in humans; it is biocompatible and biodegradable.^[38,40] Second, silk can be readily processed into many different formats, including nanoparticles that can be used for lysosomotropic drug delivery.^[41] Third, it is possible to fine tune drug release from silk.^[41,42] Furthermore, silk has remarkable properties that stabilize therapeutic proteins, as the nanocrystalline regions in the silk structure perform several functions, including providing a buffering capacity, tailoring water content at the nanoscale and providing physical protection (reviewed in ref. [43]).

Macrophages exposed to silk, PLGA, and silica nanoparticles showed marked deviations from the basal macrophage metabolic profile. These changes included higher glucose consumption and lactate production, suggesting increased glycolytic activity, as previously reported for macrophages exposed to ultrasmall superparamagnetic particles of iron oxide (USPIOs),^[17] airborne particulate matter,^[44] or bacterial lipopolysaccharide.^[13,45] The TCA cycle was also clearly affected, especially upon exposure to PLGA nanoparticles, as indicated by significant increases in itaconate and succinate (Figure 9). Itaconate has been identified in lipopolysaccharide-activated (M1) macrophages^[13,28] and is generated by the decarboxylation of the citrate-derived metabolite cis-aconitate,^[46] following a TCA cycle breakpoint at isocitrate dehydrogenase.^[47] The functional role of this metabolite has not been fully elucidated, but it is thought to be an important mediator of the immune defense mounted by macrophages.^[48] Succinate, which is known to have a proinflammatory role,^[49] is also elevated in M1 macrophages,^[13] likely in relation to a second TCA cycle breakpoint at succinate dehydrogenase.^[47] The observed changes in metabolism suggest a M1-like macrophage phenotype. Upregulation of CD80 expression and cytokine levels (Figures 2 and 8) strongly supported the notion that these nanoparticles induced metabolic reprogramming through M1-like macrophage activation. Conceivably, the significant differences in CD80 upregulation and TNF- α secretion seen in response to nanoparticle treatment could have arisen in part due to macrophage heterogeneity, and the extent of activation (i.e., the signaling threshold) quite likely determined the overall biological performance.^[50] For example, TNF- α release is influenced by many factors (e.g., material, dose, particle size, etc.); thus, the differences observed here simply serve as an overall performance indicator.^[21,25] We

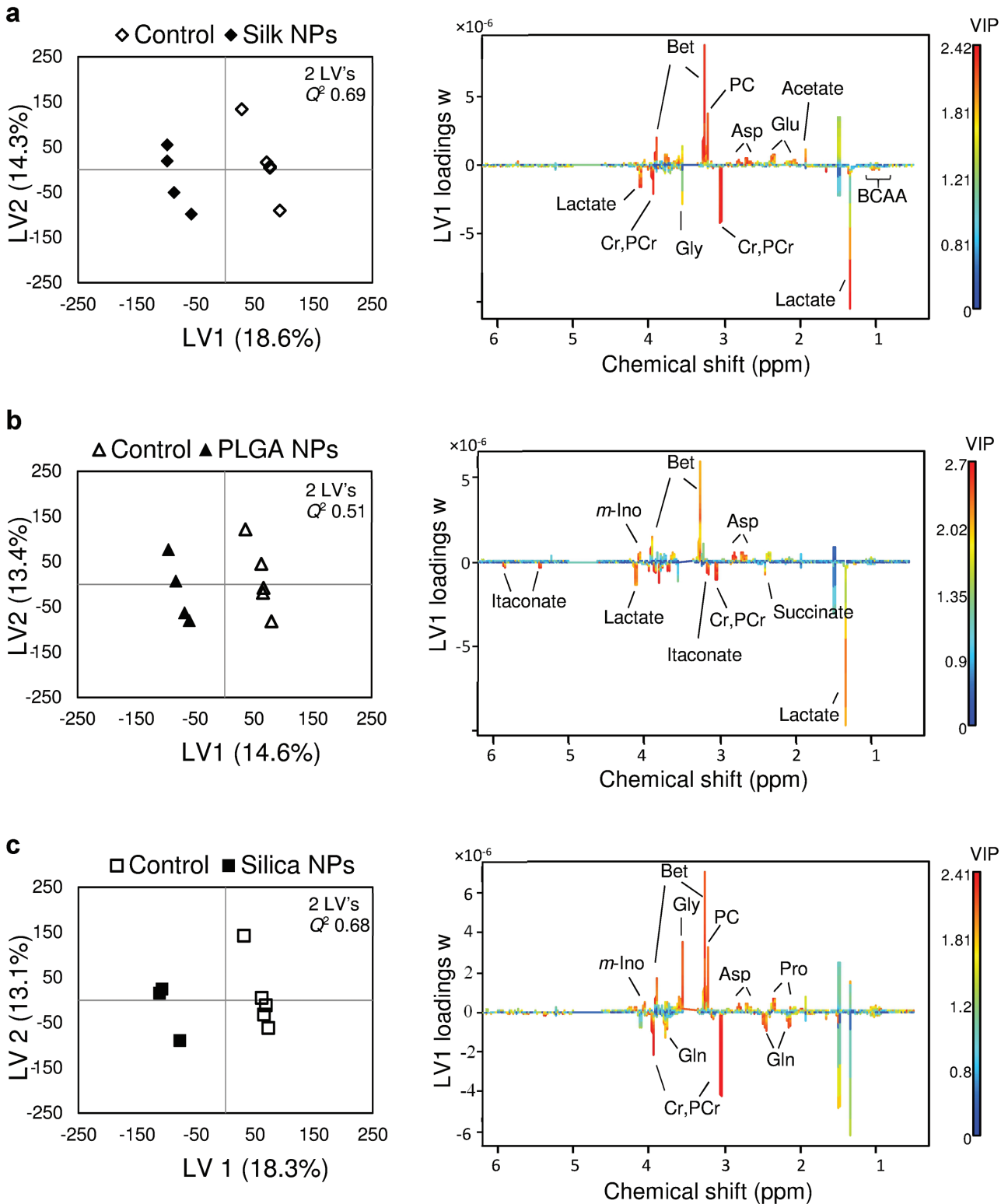


Figure 5. Multivariate analysis of ^1H NMR spectra from aqueous extracts of control cells and cells exposed for 24 h to a) silk nanoparticles, b) PLGA nanoparticles, or c) silica nanoparticles: partial-least squares discriminant analysis (PLS-DA) scores scatter plots (left) and LV1 loadings w colored as a function of variable importance in the projection (right).

speculate that the differences in $\text{TNF-}\alpha$ are due to the material per se, because we controlled the nanoparticle size, shape, and concentration.

The nanoparticles tested caused profound changes in the levels of several amino acids. Aspartate and glutamate, and to a lesser extent alanine and threonine, were consistently

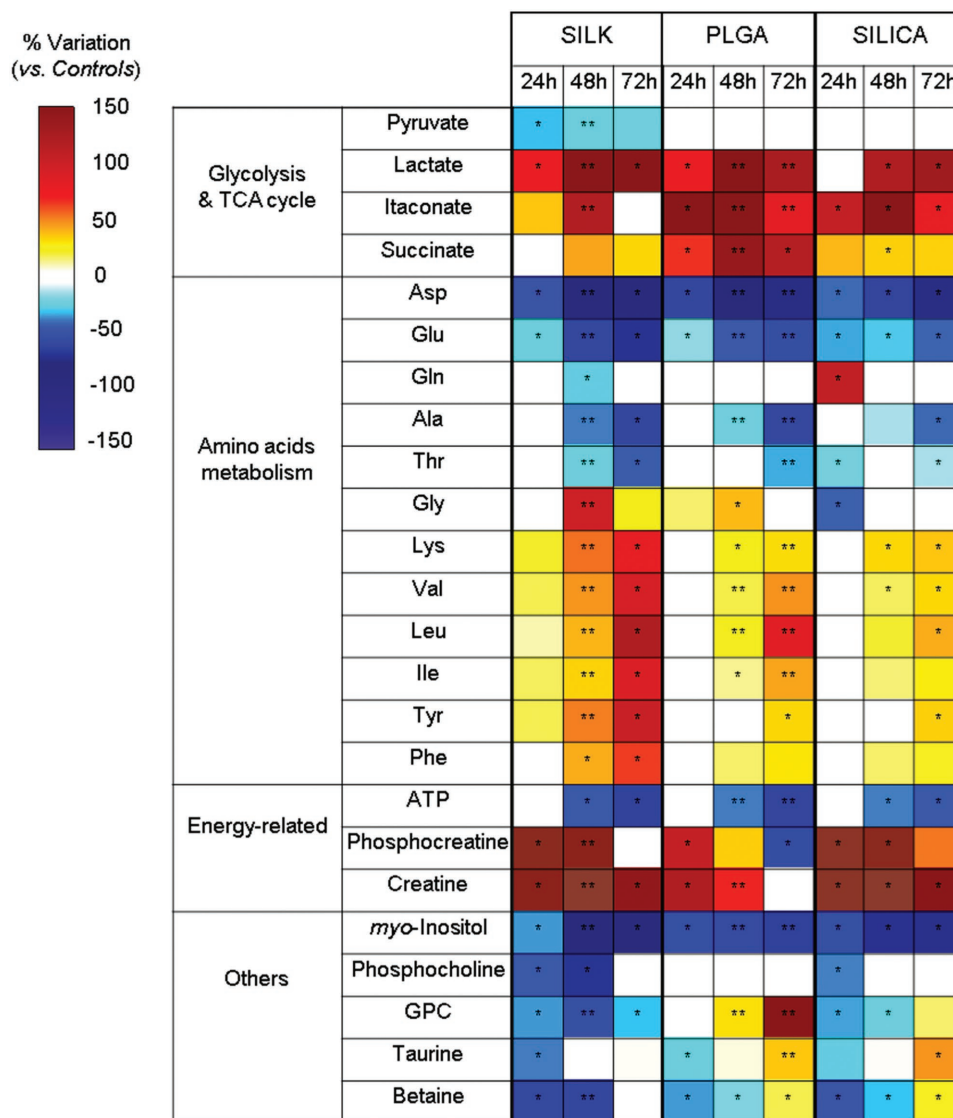


Figure 6. Heatmap of main metabolite variations in aqueous extracts of cells exposed to silk, PLGA or silica nanoparticles ($500 \mu\text{g mL}^{-1}$) for different time periods (24, 48, and 72 h), in relation to controls (color scale reflecting % variation). The criterion for including a metabolite in the heatmap was absolute effect size >0.8 (and standard error $<$ effect size). Statistically significant differences are indicated ($*p < 0.05$, $**p < 0.01$).

decreased in exposed macrophages, regardless of the nanoparticle type. This could reflect their use in replenishing the TCA cycle, namely through the aspartate arginosuccinate shunt (Figure 9). Indeed, this pathway has been shown to fuel the reprogrammed TCA cycle of inflammatory macrophages, playing an important role in their effector functions.^[47] Our results also showed that exposed macrophages consumed less glutamine from the medium when compared to control cells. This contrasts with the results reported for lipopolysaccharide-stimulated macrophages, where glutamine influx and oxidation were increased,^[13] but agrees with a recent study where M1 macrophages showed reduced glutaminolysis.^[45] Interestingly, our data further suggested that the effect of nanoparticle exposure on intracellular glutamine metabolism depended on the nanoparticle type: macrophages exposed to silk for 48 h showed decreased glutamine levels, whereas those exposed to

silica for 24 h presented higher levels of this amino acid; PLGA nanoparticles had no effect on glutamine levels. The variations in glycine levels were also suggestive of nanoparticle-specific effects. We speculate that intracellular proteolytic degradation of silk nanoparticles is responsible for the increase in glycine because glycine makes up nearly 50% of silk fibroin.^[51] However, we currently have no experimental proof for this explanation. All tested nanoparticles induced increases in lysine, branched chain, and aromatic amino acids, which could possibly reflect autophagic protein degradation. Indeed, a variety of nanoparticles have been shown to induce autophagy, leading either to increased cell death or, paradoxically, to promotion of cell survival.^[52]

In the current study, cellular ATP levels were maintained in the first 24 h of exposure but these levels decreased with longer incubations and with all nanoparticle types. This is consistent

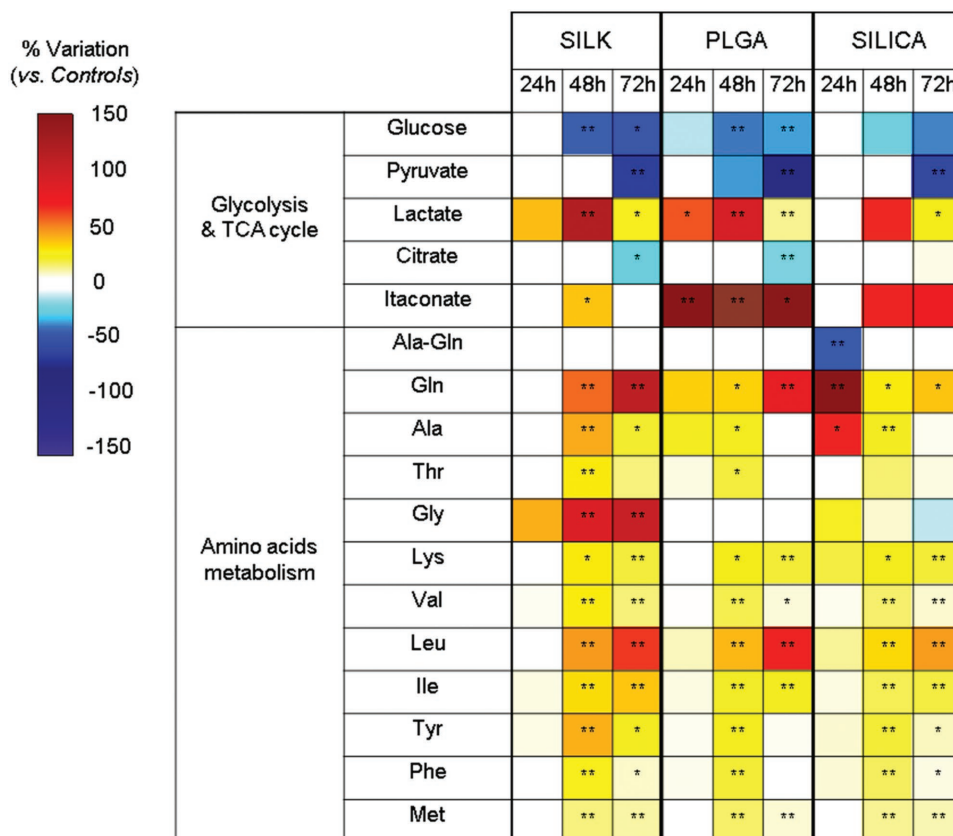


Figure 7. Heatmap of main metabolite variations in the culture medium of cells exposed to silk, PLGA or silica nanoparticles ($500 \mu\text{g mL}^{-1}$) for different time periods (24, 48, and 72 h), in relation to controls (color scale reflecting % variation). The criterion for including a metabolite in the heatmap was absolute effect size >0.8 (and standard error $<$ effect size). Statistically significant differences are indicated ($*p < 0.05$, $**p < 0.01$).

with the TCA cycle reprogramming described above: first, the inhibition of succinate dehydrogenase (complex II of the respiratory chain) is expected to decrease ATP generation through oxidative phosphorylation;^[10] second, as recently shown for lipopolysaccharide-activated macrophages, the itaconate produced by exposed macrophages could abolish mitochondrial substrate-level phosphorylation.^[48] Our results further showed huge (up to sixfold) increases in creatine and phosphocreatine in cells exposed for 24 or 48 h, followed by a lower increase or even a decrease at 72 h (depending on the nanoparticle type). Increases in these metabolites were also reported in macrophages activated with lipopolysaccharide^[53] or exposed to ultrasmall superparamagnetic particles of iron oxide.^[17] Phosphocreatine is a reusable high energy phosphate reservoir and becomes particularly important in situations of high metabolic demand, when the rate of ATP use exceeds its generation by other metabolic pathways.^[54] Early work has shown that the differentiation of monocytes into macrophages is accompanied by the expression of creatine kinase and the development of a large phosphocreatine pool,^[55] which is rapidly used up during phagocytosis.^[56] Hence, our results suggest that macrophages stimulated by nanoparticles rely on the creatine kinase/phosphocreatine system for energy buffering, maintenance of cellular homeostasis and phagocytic function.

Noticeable changes occurred in common osmolytes and/or membrane-related compounds. The decrease in myo-inositol—

observed for all nanoparticles and time points and previously reported in macrophages exposed to particulate matter^[44]—may reflect the role of this metabolite is osmoregulation and/or in phosphoinositide turnover and cell signaling. Membrane modification was further supported by decreases in phosphocholine and glycerophosphocholine levels in cells exposed to silk or silica nanoparticles, in accordance with observations made for USPIO-exposed macrophages.^[17] PLGA nanoparticles did not affect phosphocholine levels and caused an increase in glycerophosphocholine, which may also act as osmoprotectant, in agreement with the less substantial interaction of these particles with the plasma membrane observed by scanning electron microscopy. The initial decrease in taurine and betaine, followed by an increase at 72 h, could reflect the role of these metabolites in maintaining the osmotic balance, as well as their antioxidant activity. Indeed, taurine is especially abundant in inflammatory cells, such as activated macrophages, where it provides protection during processes that generate oxidants.^[57] This is plausible because a nanoparticle-mediated M1-like phenotype was observed here.

4. Conclusion

We assessed the metabolomic response of macrophages toward silk, PLGA, and silica nanoparticles that are in preclinical

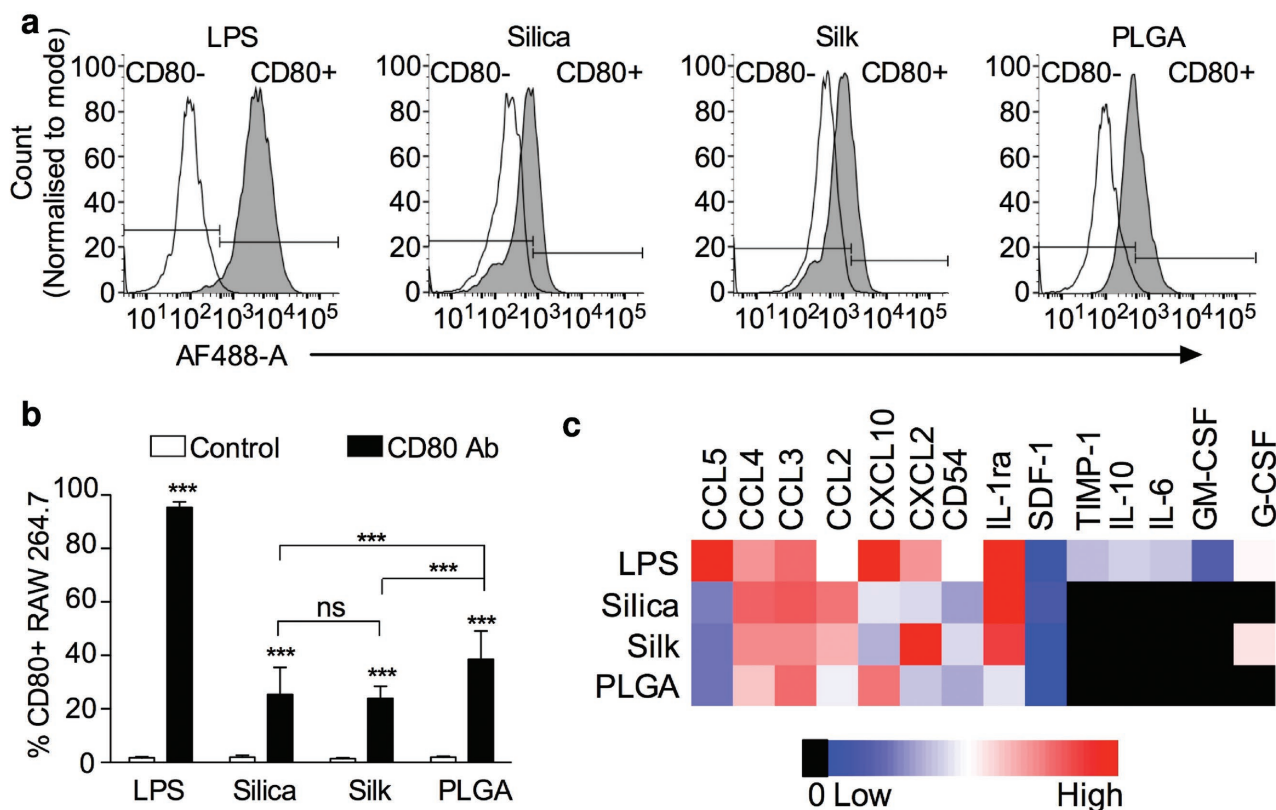


Figure 8. Nanoparticle induced M1-like macrophage phenotype. a) Plasma membrane expression of CD80, b) percentage CD80 positive macrophages, and c) expression of cytokines in response to stimuli. All data for 24 h exposure to $500 \mu\text{g mL}^{-1}$ nanoparticles and 100 ng mL^{-1} LPS, respectively. Statistically significant differences are indicated ($n = 3, \pm \text{SD}$) (** $p < 0.001$).

and clinical development for drug delivery applications. The observed upregulation of glycolysis, altered TCA cycle activity (with increased production of itaconate and succinate, and activation of amino acid catabolic routes) together with reduced ATP generation were consistent with a proinflammatory M1-like phenotype. Furthermore, aminoacids possibly derived from autophagy, the creatine kinase/phosphocreatine system and a few metabolites acting as osmolytes and/or antioxidants emerged as important players in the metabolic reprogramming of macrophages exposed to nanoparticles. This metabolic signature was a common response to all nanoparticles tested; however, the direction and magnitude of some variations were clearly nanoparticle specific, indicating material-induced biological specificity. Further metabolomic changes are also expected once a payload is added to the carrier.^[58] Overall, this study provides a benchmark for metabolic changes induced by unmodified silk, PLGA, and silica nanoparticles, and demonstrates the value of NMR metabolomics to assess nanoparticle-induced metabolic reprogramming of macrophages.

5. Experimental Section

Preparation and Characterization of Nanoparticles: *Bombyx mori* silk was extracted from cocoons and used to manufacture silk nanoparticles, as described previously;^[41,59] silk nanoparticle manufacture is presented in video format in ref. [60]. Briefly, cocoons were cut into $5 \times 5 \text{ mm}$ pieces,

degummed for 60 min and the resulting silk fibres were rinsed in ddH₂O and air dried. The fibres were then dissolved in 9.3 M LiBr solution at 60 °C for 4 h. This solution was dialyzed (molecular weight cut off 3500) against ddH₂O to remove the LiBr salt. The resulting aqueous silk solution was cleared by centrifugation and the aqueous silk (5 wt%) solution was added dropwise (20 μL per drop) to acetone, maintaining a >75% v/v acetone volume. The precipitated silk was then centrifuged, the supernatant was aspirated, and the pellet was resuspended in ddH₂O. After vortexing, the suspension was sonicated twice for 30 s at 30% amplitude with a Sonoplus HD 2070 sonicator (ultrasonic homogenizer, Bandelin, Berlin, Germany). The centrifugation, washing, and resuspension steps for the silk nanoparticle preparation were repeated at least twice more. The final silk nanoparticles were $104 \pm 1.7 \text{ nm}$ in size and had a zeta potential of -56 mV , determined by dynamic light scattering (Zetasizer Nano-ZS Malvern Instrument, Worcestershire, U.K.) in ddH₂O, as detailed previously.^[59] The silk nanoparticles were stored at 4 °C until use. PLGA ($124 \pm 0.05 \text{ nm}$, Phosphorex, Hopkinton, MA, USA) and amine-surface modified silica particles ($101 \pm 7.4 \text{ nm}$, NanoComposix San Diego, CA, USA) were purchased and used as supplied. All cell culture studies used 10 mg mL^{-1} nanoparticle stocks prepared in ddH₂O and then diluted in cell culture medium as indicated.

Scanning Electron Microscopy: The nanoparticles were visualized by scanning electron microscopy, as detailed previously.^[59] Nanoparticles were diluted with distilled water to a concentration of 1 mg mL^{-1} . The samples were then pipetted onto a silicon wafer and lyophilized overnight. The specimens were sputter coated with a 20 nm layer of gold using an ACE200 low vacuum sputter coater (Leica Microsystems, Wetzlar, Germany) and analyzed with an FE-SEM SU6600 (Hitachi High Technologies, Krefeld, Germany) at 5 kV and a 40 000-fold magnification. Cell imaging studies were conducted on RAW 264.7 cells seeded onto

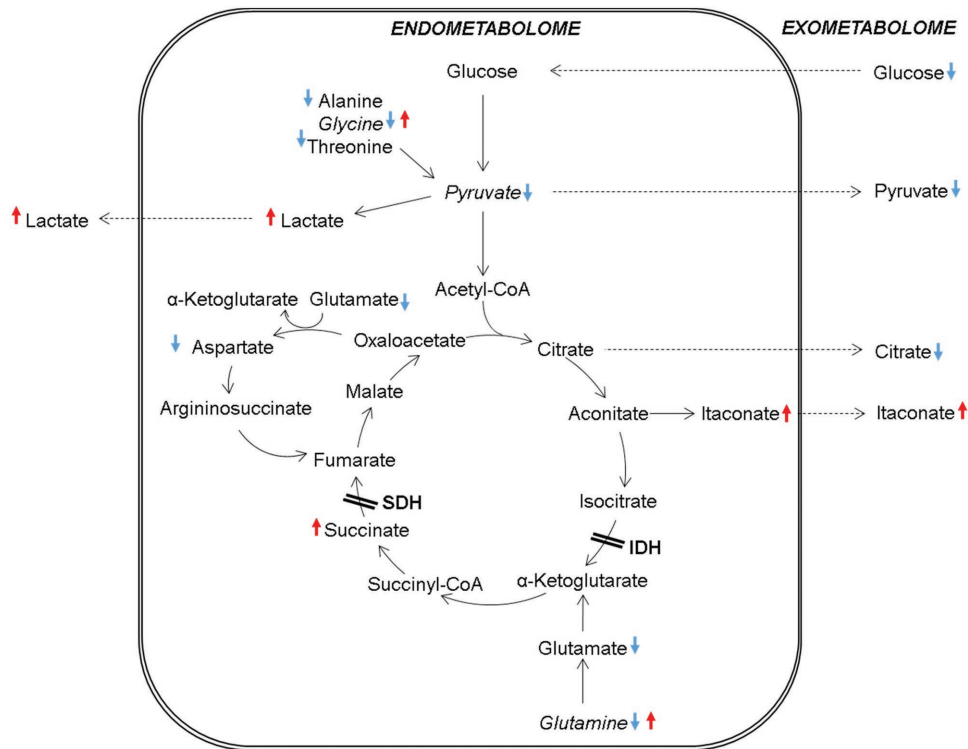


Figure 9. Diagram of main metabolic changes reflecting reprogramming of glycolysis and the TCA cycle in macrophages exposed to nanoparticles. The arrows indicate increases/decreases in relation to control cells. Metabolites in italic showed nanoparticle-dependent variations. IDH, isocitrate dehydrogenase; SDH, succinate dehydrogenase.

glass coverslips and incubated overnight as detailed below. Cells were then exposed to the desired treatments for 24 h, followed by fixation with 2% v/v glutaraldehyde in phosphate buffer saline (PBS), washing with ddH₂O twice, dehydration with an increasing ethanol series, and critical point drying (EM CPD300, Leica Microsystems, Wetzlar, Germany), as detailed elsewhere.^[61] Samples were then sputter-coated with gold and analyzed by scanning electron microscopy at 5 kV at 2500, 3500, and 4500-fold magnification.

Routine Cell Culture Maintenance: The murine macrophage RAW 264.7 cell line was purchased from ATCC (Manassas, VA, USA). Cells were cultured in Dulbecco's Modified Eagle Medium (containing 4.5 g glucose, 110 mg sodium pyruvate, 10% v/v fetal bovine serum) in a humidified 5% CO₂ atmosphere at 37 °C. The cultures were routinely subcultured every 2–3 d (when they reached 80% confluency) by scraping the cells off the flask and replating them at a split ratio of 2:10 on tissue culture-treated polystyrene (Corning, New York, NY, USA), unless otherwise stated. For nanoparticle macrophage studies cells were routinely seeded at a density of 1.5 × 10⁴ cells cm⁻². All cell culture studies were performed in accordance with the best practice guidelines;^[62] here, the cells were cultured for up to ten passages and then replaced with a new validated cryostock.

Tumor Necrosis Factor Alpha (TNF-α) Assay: Macrophage TNF-α release was assessed as detailed previously.^[59] Briefly, RAW 264.7 cells were seeded and allowed to recover overnight, as described above. The culture medium was then aspirated and replaced with fresh medium containing either (i) 15 ng of lipopolysaccharide (Sigma-Aldrich, St. Louis, MO, USA), (ii) control medium, or (iii) nanoparticles made of silk, PLGA or silica at concentrations of 10 μg mL⁻¹, and 500 μg mL⁻¹. Cultures were incubated for 24 h and then the medium was collected and centrifuged at 6000 × g for 5 min. Assay samples were stored at -80 °C and analyzed using a mouse TNF-α DuoSet ELISA (R&D Systems, Minneapolis, MN, USA), according to the manufacturer's instructions. Data were analyzed using GraphPad Prism 5.0b (GraphPad

Software, La Jolla, CA, USA). Sample pairs were analyzed with the Student's *t* test. Multiple samples were evaluated by one-way analysis of variance (ANOVA) followed by Bonferroni's multiple comparison post hoc test or the Dunnett's post hoc tests to evaluate the statistical differences between the samples and controls.

Assessment of Macrophage Activation: Cells were seeded and allowed to recover overnight as detailed above. Next, cultures were incubated with nanoparticles (500 μg mL⁻¹) for 24 h and then the cells were placed on ice, detached by scraping, harvested into 5 mL falcon tubes and centrifuged at 350 × g at 4 °C for 5 min. Tubes were placed on ice, the supernatant was discarded and cells were resuspended in either (i) control cell staining buffer (1 × PBS, 1% BSA), or (ii) cell staining buffer containing Alexa Fluor 488 (AF488) antimouse CD80 (Biolegend, San Diego, CA, USA, Clone 16-10A1) or AF488 Armenian Hamster IgG Isotype Control (Biolegend, Clone HTK888) for 20 min in the dark. Cells were then washed 3× in cell staining buffer by centrifugation and resuspended in cell staining buffer prior to data acquisition on a BD FACSCanto (Becton Dickinson, San Jose, CA, USA). Flow cytometry data were acquired using BD FACSDiva software (Becton Dickinson, San Jose, CA, USA) and analyzed using FlowJo v10.1 (TreeStar, San Carlos, CA, USA). All flow cytometry histograms and CD80 population values were obtained using FlowJo. Proteome profilers (mouse cytokine array Panel A, R&D Systems, Minneapolis, MN, USA) were used according to the manufacturer's instructions using 24 h conditioned medium (nanoparticles 500 μg mL⁻¹ and 100 ng mL⁻¹ LPS). For the analysis of arrays, blots were threshold adjusted and analyzed using ImageJ 1.38 (National Institutes of Health, Bethesda, USA).

Sample Collection for Metabolomics: For metabolomics studies RAW 264.7 cells were seeded as detailed above and allowed to recover overnight. The cells were then exposed to low (10 μg mL⁻¹) and high (500 μg mL⁻¹) nanoparticle concentrations for up to 72 h. Cell extracts were prepared as detailed elsewhere.^[63] Briefly, at the desired time points, cells were placed on ice and kept at 4 °C throughout. The culture medium was collected,

clarified by centrifugation, lyophilized and stored at -80°C until further use. The cells were washed with ice-cold PBS, quenched by addition of $650\ \mu\text{L}$ methanol 80% v/v cooled to -20°C , scraped off the dish and collected in an Eppendorf tube. Next, $260\ \mu\text{L}$ of CHCl_3 at -20°C was added to the tube and vortexed, followed by addition of $260\ \mu\text{L}$ of -20°C cooled CHCl_3 and $220\ \mu\text{L}$ of dH_2O to each sample. The samples were vortexed, allowed to rest on ice for 10 min, and then centrifuged at $2000 \times g$ for 15 min. The aqueous and lipid phases were collected; the aqueous sample was dried under a stream of N_2 and the organic phase was allowed to evaporate in a fume hood. All samples were stored at -80°C until analysis.

NMR Spectroscopy: NMR analyses were conducted on dried medium samples and aqueous extracts after reconstitution in $600\ \mu\text{L}$ of deuterated phosphate buffer ($100 \times 10^{-3}\ \text{M}$, pH 7.4) containing $0.1 \times 10^{-3}\ \text{M}$ 3-(trimethylsilyl)propionate sodium salt, (TSP)- d_4 . A $550\ \mu\text{L}$ volume of each sample was transferred into 5 mm NMR tubes. NMR spectra were acquired on a Bruker Avance DRX-500 spectrometer operating at $500.13\ \text{MHz}$ for ^1H observation, at $298\ \text{K}$, using a 5 mm probe. Standard 1D ^1H spectra with water presaturation (pulse program “noesypr1d” in the Bruker library) were recorded with a $7002.8\ \text{Hz}$ spectral width, 32 k data points, a 4 s relaxation delay and 256 scans. Spectral processing comprised exponential multiplication with $0.3\ \text{Hz}$ line broadening, zero filling to 64 k data points, manual phasing, baseline correction, and chemical shift calibration to the TSP signal at 0 ppm. 2D ^1H - ^1H total correlation (TOCSY) spectra, ^1H - ^{13}C heteronuclear single quantum correlation spectra, and J-resolved spectra were also registered for selected samples to assist spectral assignment. The main acquisition and processing parameters for these experiments are provided in Table S4 (Supporting Information).

Spectral Assignment: Metabolites were identified with the aid of 2D spectra (Figure S5, Supporting Information) and the spectral reference databases BBIREFCODE-2-0-0 (Bruker Biospin, Rheinstetten, Germany) and HMDB.^[64] The changes in RAW 264.7 conditioned medium in response to nanoparticles were assessed by establishing baseline values for tissue culture substrate conditioned medium and for RAW 264.7 conditioned medium (i.e., in the absence of nanoparticles). These control baseline data sets were then used to identify nanoparticle-specific changes in the conditioned culture medium. Also, medium samples incubated with nanoparticles (without cells) were analyzed to discard changes caused by direct interaction of nanoparticles with medium components.

Multivariate Analysis and Spectral Integration of NMR Spectra: Spectra were exported from Amix-Viewer (version 3.9.14, BrukerBiospin, Rheinstetten) and normalized by total spectral area. Using SIMCA-P 11.5 software (Umetrics, Umeå, Sweden), the resulting data were scaled to Unit Variance (UV), giving equal variance to all variables. PCA and PLS-DA were then applied after exclusion of suppressed water and contaminant signals (e.g., methanol, chloroform), with a sevenfold internal cross validation, from which Q^2 and R^2 values, reflecting predictive capability and explained variance, respectively, were extracted (SIMCA-P 11.5, Umetrics, Sweden). Selected signals in the 1D spectrum were integrated using Amix-Viewer (version 3.9.14, BrukerBiospin, Rheinstetten) and normalized by the total spectral area.

For each metabolite, the percentage variation in nanoparticle-exposed samples was calculated relative to controls, together with the effect size adjusted for small sample numbers, and the respective standard errors.^[27] The metabolite variations of large magnitude, i.e., with an absolute effect size greater than 0.8,^[27] were expressed in a heatmap colored as a function of % variation using the R-statistical software. The difference between the means of two groups (control and exposed) was assessed using the nonparametric Wilcoxon rank sum test with continuity correction (confidence level 95%).

Supporting Information

Supporting Information is available from the Wiley Online Library or from the author. All data supporting this research are openly available from <http://dx.doi.org/10.15129/39e5d0a1-65e7-4148-9990-32cb0f40d586>.

Acknowledgements

This research was supported by a Research and Development Grant (No. 1715) from the University of Strathclyde (F.P.S. and I.F.D.) and by Marie Curie FP7 Career Integration Grant (No. 334134) (NanoTrac) within the seventh European funding programme (F.P.S.). J.D.T.’s Ph.D. studentship was supported through the EPSRC Doctoral Training Partnership (EP/M508159/1), University of Strathclyde. T.W.’s Ph.D. studentship was supported through a Collaborative International Research Programme: University of Strathclyde and Nanyang Technological University, Singapore. The authors would like to acknowledge that this work was carried out in part at the CMAC National Facility, supported by a UK Research Partnership Fund award from the Higher Education Funding Council for England (Grant HH13054). The work was also developed in the scope of the project CICECO-Aveiro Institute of Materials, POCI-01-0145-FEDER-007679 (FCT Ref. UID/CTM/50011/2013), financed by national funds through the FCT/MEC and when appropriate cofinanced by FEDER under the PT2020 Partnership Agreement. The authors also acknowledge the Portuguese National NMR (PTNMR) Network, supported with FCT funds, Dr. Manfred Spraul, Bruker BioSpin (Germany), for providing access to NMR software and database, and Dr. Joana Carrola for technical support. I.F.D. further acknowledges FCT/MCTES for a research contract under the Program “Investigador FCT” 2014.

F.P.S. and I.F.D. conceived the study. R.S. acquired, analyzed, and interpreted NMR data, T.W. manufactured and characterized silk nanoparticle as well as performed electron microscopy studies, F.P.S. performed cell culture studies and J.D.T. performed flow cytometry studies. All authors (R.S., T.W., J.D.T., B.F.J., F.P.S., and I.F.D.) designed research, discussed the results, and/or advised on the analysis. F.P.S. and I.F.D. wrote the manuscript with support from the other authors.

Keywords

macrophages, NMR metabolomics, PLGA nanoparticles, silica nanoparticles, silk nanoparticles

Received: November 4, 2016

Revised: February 28, 2017

Published online: May 8, 2017

- [1] R. Duncan, R. Gaspar, *Mol. Pharm.* **2011**, *8*, 2101.
- [2] C. Sheridan, *Nat. Biotechnol.* **2012**, *30*, 471.
- [3] H. Maeda, H. Nakamura, J. Fang, *Adv. Drug Delivery Rev.* **2013**, *65*, 71.
- [4] Y. Matsumura, H. Maeda, *Cancer Res.* **1986**, *46*, 6387.
- [5] K. M. Pondman, M. Sobik, A. Nayak, A. G. Tsolaki, A. Jäkel, E. Flahaut, S. Hampel, B. Haken, R. B. Sim, U. Kishore, *Nanomedicine* **2014**, *10*, 1287.
- [6] M. M. Markiewski, R. A. DeAngelis, F. Benencia, S. K. Ricklin-Lichtsteiner, A. Koutoulaki, C. Gerard, G. Coukos, J. D. Lambris, *Nat. Immunol.* **2008**, *9*, 1225.
- [7] M. A. Miller, Y.-R. Zheng, S. Gadde, C. Pfirschke, H. Zope, C. Engblom, R. H. Kohler, Y. Iwamoto, K. S. Yang, B. Askevold, N. Kolishetti, M. Pittet, S. J. Lippard, O. C. Farokhzad, R. Weissleder, *Nat. Commun.* **2015**, *6*, 8692.
- [8] M. Niu, S. Valdes, Y. W. Naguib, S. D. Hursting, Z. Cui, *Mol. Pharm.* **2016**, *13*, 1833.
- [9] D. R. Getts, R. L. Terry, M. T. Getts, C. Deffrasnes, M. Müller, C. van Vreden, T. M. Ashhurst, B. Chami, D. McCarthy, H. Wu, J. Ma, A. Martin, L. D. Shae, P. Witting, G. S. Kansas, J. Kühn, W. Hafezi, I. L. Campbell, D. Reilly, J. Say, L. Brown, M. Y. White, S. J. Cordwell, S. J. Chadban, E. B. Thorp, S. Bao, S. D. Miller, N. J. C. King, *Sci. Transl. Med.* **2014**, *6*, 219ra7.

- [10] K. C. El Kasmi, K. R. Stenmark, *Semin. Immunol.* **2015**, *27*, 267.
- [11] E. L. Mills, L. A. O'Neill, *Eur. J. Immunol.* **2016**, *46*, 13.
- [12] J. C. Rodríguez-Prados, P. G. Través, J. Cuenca, D. Rico, J. Aragonés, P. Martín-Sanz, M. Cascante, L. Boscá, *J. Immunol.* **2010**, *185*, 605.
- [13] J. Meiser, L. Krämer, S. C. Sapcariu, N. Battello, J. Ghelfi, A. F. D'Herouel, A. Skupin, K. Hiller, *J. Biol. Chem.* **2016**, *291*, 3932.
- [14] I. F. Duarte, *J. Controlled Release* **2011**, *153*, 34.
- [15] D. S. Wishart, *Nat. Rev. Drug Discovery* **2016**, *15*, 473.
- [16] M. Lv, W. Huang, Z. Chen, H. Jiang, J. Chen, Y. Tian, Z. Zhang, F. Xu, *Bioanalysis* **2015**, *7*, 1527.
- [17] J. Feng, J. Zhao, F. Hao, C. Chen, K. Bhakoo, H. Tang, *J. Nanopart. Res.* **2011**, *13*, 2049.
- [18] L. Xiao, G. Lu, Q. Lu, D. L. Kaplan, *ACS Biomater. Sci. Eng.* **2016**, *2*, 2050.
- [19] S. Sharma, A. Parmar, S. Kori, R. Sandhir, *Trends Anal. Chem.* **2016**, *80*, 30.
- [20] A. Bitar, N. M. Ahmad, H. Fessi, A. Elaissari, *Drug Discovery Today* **2012**, *17*, 1147.
- [21] S. Bancos, D. L. Stevens, K. M. Tyner, *Int. J. Nanomedicine* **2015**, *10*, 183.
- [22] J. Meng, X. Li, C. Wang, H. Guo, J. Liu, H. Xu, *ACS Appl. Mater. Interfaces* **2015**, *7*, 3180.
- [23] T. Kusaka, M. Nakayama, K. Nakamura, M. Ishimiya, E. Furusawa, K. Ogasawara, *PLoS One* **2014**, *9*, e92634.
- [24] R. Kalluru, F. Fenaroli, D. Westmoreland, L. Ulanova, A. Maleki, N. Roos, M. Paulsen Madsen, G. Koster, W. Egge-Jacobsen, S. Wilson, H. Roberg-Larsen, G. K. Khuller, A. Singh, B. Nyström, G. Griffiths, *J. Cell Sci.* **2013**, *126*, 3043.
- [25] V. Thomas, B. A. Halloran, N. Ambalavanan, S. A. Catledge, Y. K. Vohra, *Acta Biomater.* **2012**, *8*, 1939.
- [26] K. M. Waters, L. M. Masiello, R. C. Zangar, B. J. Tarasevich, N. J. Karin, R. D. Quesenberry, S. Bandyopadhyay, J. G. Teeguarden, J. G. Pounds, B. D. Thrall, *Toxicol. Sci.* **2009**, *107*, 553.
- [27] L. Berben, S. M. Sereika, S. Engberg, *Int. J. Nurs. Stud.* **2012**, *49*, 1039.
- [28] C. L. Strelko, W. Lu, F. J. Dufort, T. N. Seyfried, T. C. Chiles, J. D. Rabinowitz, M. F. Roberts, *J. Am. Chem. Soc.* **2011**, *133*, 16386.
- [29] D. M. Mosser, X. Zhang, *Curr. Protoc. Immunol.* **2008**, Chapter 14, Unit 14.2.
- [30] R. Weissleder, M. Nahrendorf, M. J. Pittet, *Nat. Mater.* **2014**, *13*, 125.
- [31] J. Hrkach, D. Von Hoff, A. M. Mukkaram, E. Andrianova, J. Auer, T. Campbell, D. De Witt, M. Figa, M. Figueiredo, A. Horhota, S. Low, K. McDonnell, E. Peeke, B. Retnarajan, A. Sabnis, E. Schnipper, J. J. Song, Y. H. Song, J. Summa, D. Tompsett, G. Troiano, T. Van Geen Hoven, J. Wright, P. LoRusso, P. W. Kantoff, N. H. Bander, C. Sweeney, O. C. Farokhzad, R. Langer, S. Zale, *Sci. Transl. Med.* **2012**, *4*, 128ra39.
- [32] R. R. Castillo, M. Colilla, M. Vallet-Regí, *Expert Opin. Drug Delivery* **2017**, *14*, 229.
- [33] X. Lu, Y. Tian, Q. Zhao, T. Jin, S. Xiao, X. Fan, *Nanotechnology* **2011**, *22*, 055101.
- [34] A. Parveen, S. H. Rizvi, A. Gupta, R. Singh, I. Ahmad, F. Mahdi, A. A. Mahdi, *Cell Mol. Biol.* **2012**, *58*, 196.
- [35] S.-M. Huang, X. Zuo, J. J. Li, S. F. Y. Li, B. H. Bay, C. N. Ong, *Adv. Healthcare Mater.* **2012**, *1*, 779.
- [36] X. Lu, C. Ji, T. Jin, X. Fan, *Nanotechnology* **2015**, *26*, 175101.
- [37] F. G. Omenetto, D. L. Kaplan, *Science* **2010**, *329*, 528.
- [38] F. P. Seib, D. L. Kaplan, *Isr. J. Chem.* **2013**, *53*, 756.
- [39] T. Yucel, M. L. Lovett, D. L. Kaplan, *J. Controlled Release* **2014**, *190*, 381.
- [40] G. H. Altman, F. Diaz, C. Jakuba, T. Calabro, R. L. Horan, J. Chen, H. Lu, J. Richmond, D. L. Kaplan, *Biomaterials* **2003**, *24*, 401.
- [41] F. P. Seib, G. T. Jones, J. Rnjak-Kovacina, Y. Lin, D. L. Kaplan, *Adv. Healthcare Mater.* **2013**, *2*, 1606.
- [42] F. P. Seib, D. L. Kaplan, *Biomaterials* **2012**, *33*, 8442.
- [43] E. M. Pritchard, P. B. Dennis, F. Omenetto, R. R. Naik, D. L. Kaplan, *Biopolymers* **2012**, *97*, 479.
- [44] M. T. Santini, G. Rainaldi, A. Ferrante, R. Romano, S. Clemente, A. Motta, B. De Berardis, M. Balduzzi, L. Paoletti, P. L. Indovina, *Chem. Res. Toxicol.* **2004**, *17*, 63.
- [45] L. Liu, Y. Lu, J. Martinez, Y. Bi, G. Lian, T. Wang, S. Milasta, J. Wang, M. Yang, G. Liu, D. R. Green, R. Wang, *Proc. Natl. Acad. Sci. USA* **2016**, *113*, 1564.
- [46] A. Michelucci, T. Cordes, J. Ghelfi, A. Pailot, N. Reiling, O. Goldmann, T. Binz, A. Wegner, A. Tallam, A. Rausell, M. Buttini, C. L. Linster, E. Medina, R. Balling, K. Hiller, *Proc. Natl. Acad. Sci. USA* **2013**, *110*, 7820.
- [47] A. K. Jha, S. C. Huang, A. Sergushichev, V. Lampropoulou, Y. Ivanova, E. Loginicheva, K. Chmielewski, K. M. Stewart, J. Ashall, B. Everts, E. J. Pearce, E. M. Driggers, M. N. Artyomov, *Immunity* **2015**, *42*, 419.
- [48] B. Németh, J. Doczi, D. Csete, G. Kacso, D. Ravasz, D. Adams, G. Kiss, A. M. Nagy, G. Horvath, L. Tretter, A. Mócsai, R. Csépanyi-Kömi, I. Iordanov, V. Adam-Vizi, C. Chinopoulos, *FASEB J.* **2016**, *20*, 286.
- [49] G. M. Tannahill, A. M. Curtis, J. Adamik, E. M. Palsson-McDermott, A. F. McGettrick, G. Goel, C. Frezza, N. J. Bernard, B. Kelly, N. H. Foley, L. Zheng, A. Gardet, Z. Tong, S. S. Jany, S. C. Corr, M. Haneklaus, B. E. Caffrey, K. Pierce, S. Walmsley, F. C. Beasley, E. Cummins, V. Nizet, M. Whyte, C. T. Taylor, H. Lin, S. L. Masters, E. Gottlieb, V. P. Kelly, C. Clish, P. E. Auron, R. J. Xavier, L. A. O'Neill, *Nature* **2013**, *496*, 238.
- [50] T. Ravasi, C. Wells, A. Forrest, D. M. Underhill, B. J. Wainwright, A. Aderem, S. Grimmond, D. A. Hume, *J. Immunol.* **2002**, *168*, 44.
- [51] A. R. Murphy, D. L. Kaplan, *J. Mater. Chem.* **2009**, *19*, 6443.
- [52] O. Zabinnyk, M. Yezhelyev, O. Seleverstov, *Autophagy* **2007**, *3*, 278.
- [53] S. D. Lamour, B. S. Choi, H. C. Keun, I. Müller, J. Saric, *J. Proteome Res.* **2012**, *11*, 4211.
- [54] T. Wallimann, M. Wyss, D. Brdiczka, K. Nicolay, H. M. Eppenberger, *Biochem. J.* **1992**, *281*, 21.
- [55] J. D. Loike, V. F. Kozler, S. C. Silverstein, *J. Exp. Med.* **1984**, *159*, 746.
- [56] J. D. Loike, V. F. Kozler, S. C. Silverstein, *J. Biol. Chem.* **1979**, *254*, 9558.
- [57] J. Marcinkiewicz, A. Grabowska, J. Bereta, T. Stelmaszynska, *J. Leukocyte Biol.* **1995**, *58*, 667.
- [58] Y. Song, R. Zhao, Y. Hu, F. Hao, N. Li, G. Nie, H. Tang, Y. Wang, *J. Proteome Res.* **2015**, *14*, 5193.
- [59] T. Wongpinyochit, P. Uhlmann, A. J. Urquhart, F. P. Seib, *Biomacromolecules* **2015**, *16*, 3712.
- [60] T. Wongpinyochit, B. F. Johnston, F. P. Seib, *J. Vis. Exp.*, **2016**, *116*, e54669.
- [61] F. P. Seib, K. Muller, M. Franke, M. Grimmer, M. Bornhauser, C. Werner, *Tissue Eng., Part A* **2009**, *15*, 3161.
- [62] M. Yu, S. K. Selvaraj, M. M. Liang-Chu, S. Aghajani, M. Busse, J. Yuan, *Nature* **2015**, *520*, 307.
- [63] J. Carrola, V. Bastos, J. M. Ferreira de Oliveira, H. Oliveira, C. Santos, A. M. Gil AM, I. F. Duarte, *Arch. Biochem. Biophys.* **2016**, *589*, 53.
- [64] D. S. Wishart, T. Jewison, A. C. Guo, M. Wilson, C. Knox, Y. Liu, Y. Djoumbou, R. Mandal, F. Aziat, E. Dong, S. Bouatra, I. Sinelnikov, D. Arndt, J. Xia, P. Liu, F. Yallou, T. Bjorn Dahl, R. Perez-Pineiro, R. Eisner, F. Allen, V. Neveu, R. Greiner, A. Scalbert, *Nucleic Acids Res.* **2013**, *41*, D801.